CrystEngComm

Accepted Manuscript

This article can be cited before page numbers have been issued, to do this please use: Y. Chen, Y. Zhou, Z. Wang, M. Wang, W. Gao, Y. Zhou, M. Liu, X. Huang and H. Wu, *CrystEngComm*, 2019, DOI: 10.1039/C9CE00348G.

ROYAL SOCIETY OF CHEMISTRY

rsc.li/crystengcomm

CrystEngComm

View Article Online
DOI: 10.1039/C9CE00348G

ARTICLE

Received 00th January 20xx,
Accepted 00th January 20xx

DOI: 10.1039/x0xx00000x

www.rsc.org/

Enhanced mechanofluorochromic properties of 1,4-dihydropyridine-based fluorescence molecules caused by the introduction of halogen atoms

Yating Chen, Yibin Zhou, Zhiqiang Wang, Mengzhu Wang, Wenxia Gao, Yunbing Zhou, Miaochang Liu, Xiaobo Huang* and Huayue Wu*

Four cyano(ethoxycarbonyl)methylene-1,4-dihydropyridine (CMD) derivatives were designed and synthesized to study the influence of the halogen atoms on their mechanofluorochromic (MFC) properties. These CMD derivatives are demonstrated to have twisted molecular conformations and display aggregation-induced emission properties. In the crystalline state, the compounds adopt loose *J*–aggregations and exhibit yellow-green or green solid-state fluorescence. Upon grinding, the original samples of **CMD-H**, **CMD-F**, **CMD-Cl**, and **CMD-Br** show 21, 60, 61, and 52-nm red shift in the fluorescence spectra, respectively, revealing MFC characteristic. The MFC properties are demonstrated to be due to the crystalline-to-amorphous transition and the red shifts in the fluorescence spectra are attributed to the increased molecular conjugations by the planarization of molecular conformations. The X-ray crystallographic analyses reveal that halogen-substituted CMD derivatives have more twisted conformations and looser stacking arrangements than **CMD-H**, which is responsible for their higher contrast MFC properties. The work indicates that the introduction of halogen atoms to a specific fluorescent molecule might be used as a simple and feasible route for developing high contrast MFC-active materials.

Introduction

Mechanofluorochromic (MFC) materials refer to a kind of smart stimuli-responsive fluorescent compounds that exhibit solid-state fluorescence color and/or intensity changes upon mechanical stimuli and have drawn wide attention owing to their potential applications in mechanical sensors, security inks, and optical recording.[1] Since Sagara and Araki *et al.* reported the first pure organic compound with MFC property in 2007,[2] some organic MFC-active compounds have emerged in the past decade.[3] Generally, organic compounds that emit solid-state fluorescence and have variable aggregated states under external pressure are considered as good candidates for MFC-active materials. Most of MFC activities are demonstrated to originate from the crystalline-to-amorphous or crystalline-to-crystalline transition.[1b] Although the development of organic MFC-active molecules with novel structures is fascinating, this depends largely on accidental discovery and screening of a large number of compounds because it is difficult to predict whether a particular molecule can exhibit an obvious solid-state fluorescence response behavior under mechanical stimuli. Considering that the solid-state emission of an organic compound is closely related to their stacking arrangement,[4] the molecular conformations and intermolecular interactions of traditional fluorescent molecules can be adjusted by appropriate structural modifications to obtain variable stacking arrangements, which is of great significance for the generation of new MFC materials.

Because halogen atoms have the strong electron-withdrawing ability, introducing halogen atoms into a specific fluorescent molecule helps to regulate the intermolecular interactions and stacking arrangements, which might be beneficial for the generation or enhancement of MFC phenomena. In 2014, Lu's group investigated the effect of a bromine atom on the MFC activities of phenothiazine-based benzoxazole derivatives.[5] It was found that bromine-substituted derivative exhibited higher contrast and more stable MFC activity than the derivative without the bromine atom, which was attributed that bromine atom could result in a looser π-π stacking and a larger sliding angle. In 2015, Cheng's group reported that bromine-substituted anthracene derivative exhibited reversible MFC property, while the anthracene derivative without the bromine atom was non-MFC, which was believed that the presence of the bromine atom affected the intermolecular interactions through the formation of the non-covalent interactions between the carbon and hydrogen atoms with the bromine atom.[6] In 2016, Wei's group found that only fluorine-substituted phenothiazinyl phenylacrylonitrile derivative displayed

---

College of Chemistry and Materials Engineering, Wenzhou University, Wenzhou, 325035, P. R. China. E-mail: xiaobhuang@wzu.edu.cn; huayuewu@wzu.edu.cn

† Electronic Supplementary Information (ESI) available: Photophysical properties, XRD curves, crystal structures, ^{1}H NMR, and ^{13}C NMR. See DOI: 10.1039/x0xx00000x

View Article Online
DOI: 10.1039/C9CE00348C

an outstanding MFC phenomenon because it had better crystallinity than chlorine- and bromine-substituted derivatives.[7] In 2016, Du's group demonstrated that the introduction of the halogen atoms to the tetraphenylethylene-based difluoroboron β-diketonate derivatives could improve the contrast of the MFC phenomena and affect the reversibility by adjusting the crystallizability of the solid samples.[8] However, unlike those mentioned above, Fraser's group reported that the introduction of halogen atoms and different halogen atoms had little effect on the MFC properties of difluoroboron β-diketonate derivatives in 2015.[9] These results indicate that halogen atoms have complex influences on the MFC activity of fluorescent molecules with specific structures, and the mechanism of their actions is still unclear. The role of halogen atoms deserves further study.

1,4-Dihydropyridine is one of traditional fluorescent molecular structure units and has been proved to be used to construct molecules that emit solid-state fluorescence in recent years.[3a,10] The 1,4-dihydropyridine derivatives often exhibited aggregation-induced emission (AIE) properties because of their twisted molecular conformations induced by the introduction of various substituents into the nitrogen atom.[11] Furthermore, some of them were reported to display fluorescence stimulus-responsive activities in the solid state.[11b-g] Herein, four cyano(ethoxycarbonyl)methylene-1,4-dihydropyridine (CMD) derivatives (**CMD-H**, **CMD-F**, **CMD-Cl**, and **CMD-Br**) were designed and synthesized to study the influence of the halogen atoms on their MFC properties (Scheme 1). These CMD derivatives were demonstrated to have twisted molecular conformations by X-ray crystallographic analyses and exhibited obvious AIE activities in the aggregated state. In the crystalline state, the molecules of these compounds adopted loose *J*–aggregation and emitted yellow-green or green fluorescence. Importantly, although all CMD derivatives exhibited MFC activities upon grinding, halogen-substituted derivatives showed higher contrast than **CMD-H**, which might be attributed that the former had more twisted conformations and looser stacking arrangements caused by the introduction of halogen atoms.

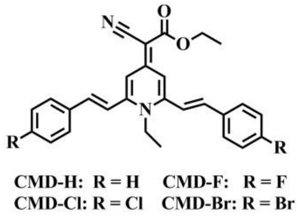

Scheme 1. Chemical structures of the CMD derivatives

Experimental

Measurements and materials

^{1}H and ^{13}C nuclear magnetic resonance (NMR) spectra were determined using a Bruker DRX 500 NMR spectrometer using dimethyl sulfoxide (DMSO)-d_6 as a solvent and trimethylsilane as a reference. Elemental analyses were recorded using an Elementar Vario MICRO analyzer. The mass spectrum was determined on a Finnigan DCMDX-30000 LCQ DCMD mass spectrometer. Fourier transform infrared (FT-IR) spectra were determined using a Nexus 870 FT-IR spectrometer. Ultraviolet-visible (UV-vis) absorption and fluorescence spectra were conducted using a Cary 500 spectrometer and a HITACHI F-4500 spectrophotometer, respectively. Solid-state fluorescence quantum yields (Φ_F) and time-resolved fluorescence decay parameters were obtained using a Fluoromax-4 spectrophotometer. X-Ray diffraction (XRD) patterns were recorded using a Rigaku Dmax 2000. The X-ray crystallographic analyses were conducted using a Bruker SMART II CCD area detector. Ethyl 2-cyanoacetate, 2,6-dimethyl-4-pyrone (**1**), acetic anhydride (Ac_2O), benzaldehyde, 4-fluorobenzaldehyde, 4-chlorobenzaldehyde, 4-bromobenzaldehyde, and ethylamine were purchased from commercial suppliers.

Synthesis of ethyl 2-cyano-2-(2,6-dimethyl-4*H*-pyran-4-ylidene)acetate (2)

Compound **1** (1.24 g, 10.0 mmol) and ethyl cyanoacetate (30.0 mmol) were dissolved in 8 mL of acetic anhydride. The mixture was heated for 3 h at 110 °C. After the reaction was over, the mixture was allowed to stand overnight, a large amount of solids separated out. After vacuum filtration, the product was washed with ethanol and then dried to afford pure compound **2** as a light brown solid (1.04 g, 47.2% yield). m. p. 187.2-187.8 °C. ^{1}H NMR (500 MHz, DMSO-d_6): δ 7.81 (s, 1H), 6.60 (s, 1H), 4.14 (q, J = 7.0 Hz, 2H), 2.35 (s, 3H), 2.33 (s, 3H), 1.22 (t, J = 7.5 Hz, 3H). ^{13}C NMR (125 MHz, DMSO-d_6): δ 164.3, 163.9, 163.3, 154.2, 118.1, 107.4, 105.7, 77.4, 59.8, 19.7, 19.4, 14.2. MS (ESI, m/z): 220.09 $[M+H]^+$.

Synthesis of compounds 3a–3d

General procedure: Compound **2** (219.2 mg, 1.0 mmol), benzaldehyde/4-fluorobenzaldehyde/ 4-chlorobenzaldehyde/4-bromobenzaldehyde (4.0 mmol) and sodium hydroxide (3.0 mmol) were dissolved in 40 mL of ethanol. The mixture was stirred at room temperature for 4 h under N_2 atmosphere. After the reaction was completed, a large amount of solids separated out. After vacuum filtration, the product was washed with water and ethanol in turn, and then dried to give pure compounds **3a**-**3d**. The characterization data of **3a**-**3d** are as follows:

Ethyl 2-cyano-2-(2,6-di((*E*)-styryl)-4*H*-pyran-4-ylidene)acetate (**3a**). Orange-yellow solid (229.8 mg), 58.1% yield, m. p. 150.6-150.7 °C. ^{1}H NMR (500 MHz, DMSO-d_6): δ 8.05 (d, J = 1.5 Hz, 1H), 7.86-7.82 (m, 4H), 7.73 (dd, ^3J = 16.0 Hz, ^4J = 5.0 Hz, 2H), 7.47-7.40 (m, 7H), 7.31 (d, J = 16.5 Hz, 1H), 4.20 (q, J = 7.0 Hz, 2H), 1.26 (t, J = 7.0 Hz, 3H). ^{13}C NMR (125 MHz, DMSO-d_6): δ 164.1, 158.3, 157.7, 152.9, 136.8, 136.4, 135.2, 135.1, 129.78, 129.75, 128.81, 128.80, 128.1, 128.0, 120.0, 119.7, 118.1, 109.1, 107.6, 79.9, 60.0, 14.2. MS (ESI, m/z): 396.36 $[M+H]^+$. Anal. calcd. for $C_{26}H_{21}NO_3$: C, 78.97; H, 5.35; N, 3.54. Found: C, 78.68; H, 5.33; N, 3.56.

Ethyl 2-(2,6-bis((*E*)-4-fluorostyryl)-4*H*-pyran-4-ylidene)-2-cyanoacetate (**3b**). Orange-yellow solid (384.4. mg), 89.1% yield, m. p. 235.2-235.5 °C. ^{1}H NMR (500 MHz, DMSO-d_6): δ 8.00 (d, J = 2.0 Hz, 1H), 7.89-7.84 (m, 4H), 7.68 (dd, ^3J = 16.0 Hz, ^4J = 5.5 Hz, 2H), 7.35-7.22 (m, 6H), 6.80 (d, J = 2.0 Hz, 1H), 4.17 (q, J = 7.0 Hz, 2H),

DOI: 10.1039/C9CE00348G

1.25 (t, *J* = 7.5 Hz, 3H). ^{13}C NMR (125 MHz, DMSO-d_6): δ 164.1, 162.90 (d, *J* = 247.5 Hz), 162.88 (d, *J* = 247.5 Hz), 158.2, 157.6, 152.9, 135.5, 135.1, 131.80 (d, *J* = 5.0 Hz), 131.77 (d, *J* = 6.3 Hz), 130.25 (d, *J* = 13.8 Hz), 130.18 (d, *J* = 13.8 Hz), 119.68 (d, *J* = 30.0 Hz), 119.67 (d, *J* = 30.0 Hz), 118.1, 115.82 (d, *J* = 21.3 Hz), 115.80 (d, *J* = 21.3 Hz), 109.0, 107.5, 79.9, 60.0, 14.2. MS (ESI, m/z): 432.11 [M+H]$^+$. Anal. calcd. for $C_{26}H_{19}F_2NO_3$: C, 72.38; H, 4.44; N, 3.25. Found: C, 72.69; H, 4.42; N, 3.23.

Ethyl 2-(2,6-bis((*E*)-4-chlorostyryl)-4*H*-pyran-4-ylidene)-2-cyanoacetate (**3c**). Orange-yellow solid (378.8 mg), 81.6% yield, m. p. 236.4-236.7 °C. ^{1}H NMR (500 MHz, DMSO-d_6): δ 8.02 (d, *J* = 1.5 Hz, 1H), 7.85-7.81 (m, 4H), 7.68 (dd, ^3J = 16.0 Hz, ^4J = 5.5 Hz, 2H), 7.52-7.50 (m, 4H), 7.42 (d, *J* = 16.0 Hz, 1H), 7.32 (d, *J* = 16.0 Hz, 1H), 6.83 (d, *J* = 15.0 Hz, 1H), 4.18 (q, *J* = 7.0 Hz, 2H), 1.25 (t, *J* = 7.0 Hz, 3H). ^{13}C NMR (125 MHz, DMSO-d_6): δ 164.0, 158.0, 157.4, 152.7, 135.3, 134.9, 134.24, 134.21, 134.1, 134.0, 129.7, 129.6, 128.83, 128.80, 120.7, 120.4, 118.0, 109.4, 107.9, 80.3, 60.1, 14.2. MS (ESI, m/z): 465.80 [M+H]$^+$. Anal. calcd. for $C_{26}H_{19}Cl_2NO_3$: C, 67.25; H, 4.12; N, 3.02. Found: C, 66.97; H, 4.10; N, 3.04.

Ethyl 2-(2,6-bis((*E*)-4-bromostyryl)-4*H*-pyran-4-ylidene)-2-cyanoacetate (**3d**). Orange-yellow solid (453.6 mg), 82.0% yield, m. p. 249.7-250.5°C. ^{1}H NMR (500 MHz, DMSO-d_6): δ 8.02 (d, *J* = 1.0 Hz, 1H), 7.78-7.74 (m, 4H), 7.69-7.63 (m, 6H), 7.44 (d, *J* = 16.0 Hz, 1H), 7.34 (d, *J* = 16.5 Hz, 1H), 4.18 (q, *J* = 7.0 Hz, 2H), 1.25 (t, *J* = 7.0 Hz, 3H). ^{13}C NMR (125 MHz, DMSO-d_6): δ 164.0, 158.0, 157.4, 152.7, 135.4, 135.0, 134.43, 134.38, 131.8, 131.7, 129.9, 129.8, 123.1, 123.0, 120.7, 120.5, 118.0, 109.4, 108.0, 80.4, 60.1, 14.2. MS (ESI, m/z): 554.31 [M+H]$^+$. Anal. calcd. for $C_{26}H_{19}Br_2NO_3$: C, 56.45; H, 3.46; N, 2.53. Found: C, 56.19; H, 3.48; N, 2.52.

Synthesis of the CMD derivatives

General procedure: Compound **3a**/**3b**/**3c**/**3d** (0.5 mmol) and ethylamine (0.8 mL) were dissolved in 6 mL of acetonitrile. The mixture was heated at 80 ° C for 6 h under N_2 atmosphere. After cooling to room temperature, the precipitate was filtered and washed with methanol, and dried to afford pure target compounds. The characterization data of **CMD-H**, **CMD-F**, **CMD-Cl**, and **CMD-Br** are as follows:

Ethyl 2-cyano-2-(1-ethyl-2,6-di((*E*)-styryl)pyridin-4(1*H*)-ylidene)acetate (**CMD**-**H**). yellow solid (122.1 mg), 57.8% yield, m. p. 274.7-275.4 °C. ^{1}H NMR (500 MHz, DMSO-d_6): δ 8.49 (d, *J* = 2.0 Hz, 1H), 7.78 (d, *J* = 7.5 Hz, 2H), 7.50-7.39 (m, 8H), 7.29 (dd, ^3J = 15.5 Hz, ^4J = 10.0 Hz, 2H), 6.98 (d, *J* = 2.0 Hz, 1H), 4.37 (q, *J* = 6.5 Hz, 2H), 4.08 (q, *J* = 7.5 Hz, 2H), 1.32 (t, *J* = 7.0 Hz, 3H), 1.21 (t, *J* = 7.0 Hz, 3H). ^{13}C NMR (125 MHz, DMSO-d_6): δ 166.3, 153.5, 148.4, 148.1, 138.2, 138.1, 135.3, 129.5, 128.83, 128.80, 127.8, 121.2, 120.8, 120.5, 112.8, 112.1, 66.8, 58.4, 44.9, 14.62, 14.55. MS (ESI, m/z): 423.40 [M+H]$^+$. FT-IR (KBr, cm^{-1}): 2988, 2186, 1672, 1637, 1618, 1601, 1534, 1472, 1379, 1269, 1052, 967, 755, 691. Anal. calcd. for $C_{28}H_{26}N_2O_2$: C, 79.59; H, 6.20; N, 6.63. Found: C, 79.27; H, 6.17; N, 6.60.

Ethyl 2-cyano-2-(1-ethyl-2,6-bis((*E*)-4-fluorostyryl)pyridin-4(1*H*)-ylidene)acetate (**CMD**-**F**). yellow-green solid (167.3 mg), 56.5% yield, m. p. 259.0-259.4 °C. ^{1}H NMR (500 MHz, DMSO-d_6): δ 8.47 (d, *J* = 2.0 Hz, 1H), 7.88-7.84 (m, 4H), 7.46-7.40 (m, 2H), 7.33-7.27 (m, 6H), 6.96 (d, *J* = 2.0 Hz, 1H), 4.36 (q, *J* = 8.5 Hz, 2H), 4.08 (q, *J* = 7.2 Hz, 2H), 1.30 (t, *J* = 7.2 Hz, 3H), 1.20 (t, *J* = 7.2 Hz, 3H). ^{13}C NMR (125 MHz, DMSO-d_6): δ 166.3, 153.4, 148.2, 147.9, 136.8, 134.3, 133.9, 129.54, 129.52, 128.82, 128.79, 121.6, 121.3, 121.2, 112.9, 112.2, 67.0, 58.5, 44.9, 14.6. MS (ESI, m/z): 459.29 [M+H]$^+$. FT-IR (KBr, cm^{-1}): 2979, 2186, 1656, 1633, 1600, 1534, 1534, 1510, 1471, 1379, 1302, 1272, 1052, 978, 852, 826. Anal. calcd. for $C_{28}H_{24}F_2N_2O_2$: C, 73.35; H, 5.28; N, 6.11. Found: C, 72.99; H, 5.30; N, 6.08.

Ethyl 2-(2,6-bis((*E*)-4-chlorostyryl)-1-ethylpyridin-4(1*H*)-ylidene)-2-cyanoacetate (**CMD**-**Cl**). yellow-green solid (122.1 mg), 68.1% yield, m. p. 246.7-247.7°C. ^{1}H NMR (500 MHz, DMSO-d_6): δ 8.47 (d, *J* = 2.0 Hz, 1H), 7.82 (d, *J* = 8.0 Hz, 4H), 7.51-7.46 (m, 6H), 7.29 (t, *J* = 15.5 Hz, 2H), 6.97 (d, *J* = 2.0 Hz, 1H), 4.35 (q, *J* = 7.0 Hz, 2H), 4.08 (q, *J* = 7.0 Hz, 2H), 1.30 (t, *J* = 7.0 Hz, 3H), 1.20 (t, *J* = 7.0 Hz, 3H). ^{13}C NMR (125 MHz, DMSO-d_6): δ 166.3, 153.4, 148.2, 147.9, 136.8, 134.3, 133.9, 129.54, 129.52, 128.82, 128.79, 121.6, 121.3, 121.2, 112.9, 112.2, 67.0, 58.5, 44.9, 14.6. MS (ESI, m/z): 492.31 [M+H]$^+$. FT-IR (KBr, cm^{-1}): 2977, 2183, 1657, 1635, 1616, 1599, 1534, 1474, 1378, 1268, 1052, 968, 815, 808. Anal. calcd. for $C_{28}H_{24}Cl_2N_2O_2$: C, 68.44; H, 4.92; N, 5.70. Found: C, 68.71; H, 4.94; N, 5.67.

Ethyl 2-(2,6-bis((*E*)-4-bromostyryl)-1-ethylpyridin-4(1*H*)-ylidene)-2-cyanoacetate (**CMD**-**Br**). yellow-green solid (195.9 mg), 67.5% yield, m. p. 246.6-247.6°C. ^{1}H NMR (500 MHz, DMSO-d_6): δ 8.47 (d, *J* = 2.0 Hz, 1H), 7.75 (d, *J* = 8.0 Hz, 4H), 7.64 (d, *J* = 8.5 Hz, 4H), 7.50 (dd, ^3J = 16.0 Hz, ^4J = 7.5 Hz, 2H), 7.28 (t, *J* = 16.0 Hz, 2H), 6.97 (d, *J* = 2.0 Hz, 1H), 4.35 (q, *J* = 7.0 Hz, 2H), 4.08 (q, *J* = 7.0 Hz, 2H), 1.29 (t, *J* = 7.0 Hz, 3H), 1.20 (t, *J* = 7.0 Hz, 3H). ^{13}C NMR (125 MHz, DMSO-d_6): δ 166.2, 153.4, 148.1, 147.8, 136.9, 134.6, 131.71, 131.69, 129.8, 129.7, 122.7, 121.7, 121.3, 121.1, 112.8, 112.2, 67.0, 58.4, 44.9, 14.6. MS (ESI, m/z): 581.02 [M+H]$^+$. FT-IR (KBr, cm^{-1}): 2985, 2204, 1698, 1641, 1616, 1546, 1511, 1487, 1318.46, 1241, 1043, 946, 851, 807. Anal. calcd. for $C_{28}H_{24}Br_2N_2O_2$: C, 57.95; H, 4.17; N, 4.83. Found: C, 58.22; H, 4.19; N, 4.80.

Results and discussion

Synthesis and characterization

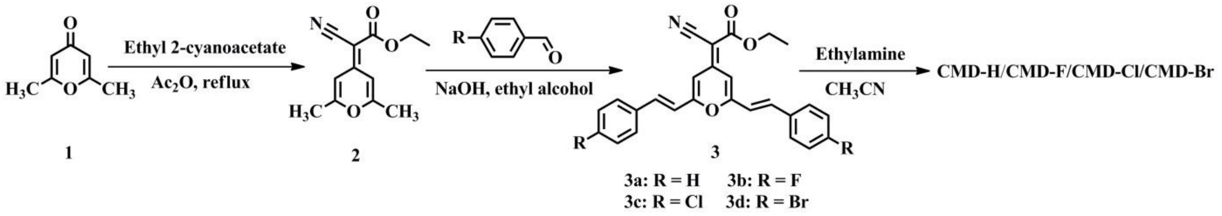

Scheme 2. Synthetic route towards the CMD derivatives

View Article Online
DOI: 10.1039/C9CE00348G

The chemical structures and synthetic routes of **CMD-H**, **CMD-F**, **CMD-Cl**, and **CMD-Br** are outlined in Scheme 2. The target compounds could be easily synthesized from a 3-step reaction procedure using compound **1** as the starting compound. Firstly, the Knoevenagel reaction of compound **1** with ethyl 2-cyanoacetate in acetic anhydride gave the intermediate **2**.[12] Secondly, intermediate **2** reacted with benzaldehyde/4-fluorobenzaldehyde/4-chlorobenzaldehyde/4-bromobenzaldehyde by an addition-elimination mechanism to afford the intermediates **3a**-**3d**, respectively. Finally, the intermediates **3a**-**3d** reacted with ethylamine to afford **CMD-H**, **CMD-F**, **CMD-Cl**, and **CMD-Br** in acetonitrile, respectively. All target compounds were fully characterized by mass spectrometry, nuclear magnetic resonance, elemental analysis, and X-ray crystallographic analyses. The target

Table 1 Crystallographic data and details of collection and refinement for crystals **CMD-H**, **CMD-F**, **CMD-Cl**, and **CMD-Br**

	CMD-H	**CMD-F**	**CMD-Cl**	**CMD-Br**
CCDC (No.)	1897635	1897637	1897636	1897638
Empirical formula	$C_{28}H_{26}N_2O_2$	$C_{28}H_{24}F_2N_2O_2$	$C_{28}H_{24}Cl_2N_2O_2$	$C_{28}H_{24}Br_2N_2O_2$
Formula weight	422.51	458.49	491.39	580.31
Temperature (K)	170.01	170.02	173(2)	173(2)
Crystal system	Orthorhombic	Monoclinic	Monoclinic	Monoclinic
Space group	*P* bca	*P*ī 2(1)/*c*1	*P* 2(1)/*c*	*P* 2(1)/*c*
Z	8	4	4	4
D_{calcd} [Mg/m^3]	1.256	1.209	1.228	1.434
F (000)	1792	960	1024	1024
ϑ range [°]	3.059-54.994	3.027-55.258	2.386-25.499	2.821- 25.499
R_1 [I>2σ(I)]	0.0926	0.0713	0.0692	0.0719
wR_2 [I>2σ(I)]	0.1703	0.2004	0.1488	0.1798
a [Å]	20.0543(6)	16.7550(8)	17.277(2)	17.384(4)
b [Å]	8.8607(3)	19.7470(10)	19.953(3)	19.973(5)
c [Å]	25.1405(8)	7.6891(4)	7.8040(11)	7.823(2)
α [deg]	90	90	90	90
β [deg]	90	98.211(3)	98.811(5)	98.170(10)
γ [deg]	90	90	90	90
V [Å^3]	4467.3(2)	2517.9(2)	2658.5(6)	2688.7(12)
GOF	1.069	1.056	1.016	1.021
R (int)	0.1373	0.0647	0.0601	0.0433
No. of reflcns collected	46033	26256	12237	10000
No. of unique reflcns	4263	4795	4884	4834
R_1 (all data)	0.1829	0.0940	0.1443	0.1311
wR_2 (all data)	0.2082	0.2190	0.1926	0.2155

View Article Online
DOI: 10.1039/C9CE00348G

compounds have good solubility in common organic solvents, such as chloroform, DMSO, dichloromethane, tetrahydrofuran, toluene, and acetonitrile, but low solubility in methanol, ethanol, and water.

Single-crystal structures

The single crystals of **CMD-H** and **CMD-F** were cultured from a slow evaporation of a DMSO/ethyl acetate (EA) (v/v = 1:1) mixture and a slow diffusion of a CHCl$_3$/methanol (v/v = 1:1) mixture, respectively. Those of **CMD-Cl** and **CMD-Br** were cultured from a slow evaporation of a CHCl$_3$/EA (v/v = 1:2) mixture. Fig. 1 shows the crystal structures and single-crystal fluorescent photographs of the target compounds. The respective crystallographic data and refinement parameters are depicted in Table 1. The single crystals of **CMD-H** and **CMD-F** belong to an orthorhombic system and a monoclinic system in a *P* bca and a $P\bar{1}$ 2(1)/*c*1 space group, respectively. The unit cells of **CMD-Cl** and **CMD-Br** are monoclinic with a *P* 2(1)/*c* space group.

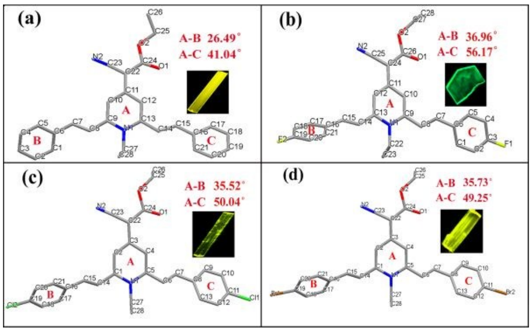

Fig. 1 Crystal structures and single-crystal fluorescent photographs of **CMD-H** (a), **CMD-F** (b), **CMD-Cl** (c), and **CMD-Br** (d).

In **CMD-H** crystal, taking the central dihydropyridine ring as the basic plane (ring A), the diheral angles between ring A and the phenyl ring B and C are 26.49° and 41.04° (Fig. 1), respectively, indicating that crystal structure adopts a twisted molecular conformation because of the introduction of the *N*-ethyl group. The distances between the central of the dihydropyridine rings in the upper and lower layers are 4.638 and 4.554 Å (Fig. 2b), indicating that there is no obvious π–π stacking. As displayed in Fig. 2 and Table 1, the molecules of **CMD-H** in the same column are stabilized by various C–H···π bonds (2.459, 3.486, 3.614, and 3.634 Å), one kind of C–H···O hydrogen bond (2.436 Å), and one kind of C–H···H interaction (2.281 Å), while those in different columns are stabilized by C–H···H interactions (2.365 and 2.391 Å) (Fig. 2c and Table 2). These multiple weak interactions cause that the molecules are aligned in a zigzag shape with a head-to-tail *J*-aggregation in the same column (Fig. 2a).

For **CMD-F**, **CMD-Cl**, and **CMD-Br**, the diheral angles between the dihydropyridine unit and the two phenyl units are 36.96° and 56.17°, 35.52° and 50.04°, 35.73° and 49.25° (Fig. 1), respectively. These results indicate that halogen-substituted CMD derivatives have more twisted conformations than **CMD-H**. Furthermore, the intermolecular interactions and stacking arrangements in the single crystals of **CMD-F**, **CMD-Cl**, and **CMD-Br** were investigated. The distances of their intermolecular interactions are listed in Table 2.

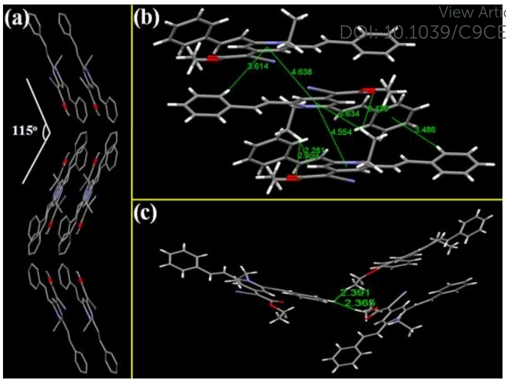

Fig. 2 Crystal **CMD-H**: (a) Molecular stacking arrangement; (b) intermolecular interactions in the same column including C–H···O hydrogen bond, C–H···π bond, and C–H···H interaction; (c) C–H···H interactions between different columns.

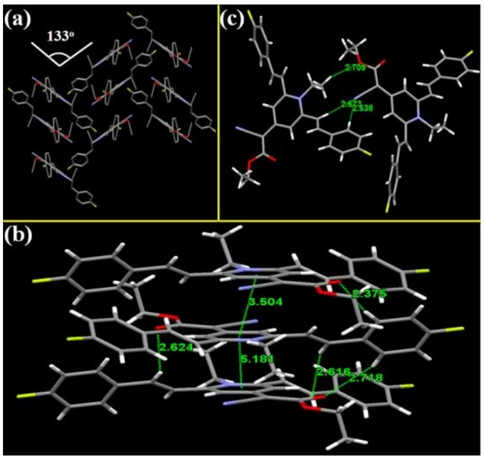

Fig. 3 Crystal **CMD-F:** (a) Molecular stacking arrangement; (b) C–H···π bond and C–H···O hydrogen bond in the same column; (c) C–H···O (N) hydrogen bonds between different columns.

The molecules of **CMD-F** in the same column are connected by C–H···π bond (2.616 Å), C–H···O hydrogen bonds (2.375, 2.624, and 2.718 Å), and π–π stacking interaction with a distance of 3.504 Å between the dihydropyridines (Fig. 3b). The molecules in different columns are connected by C–H···N hydrogen bonds (2.538 and 2.673 Å) and C–H···O hydrogen bond (2.709 Å) (Fig. 3c). **CMD-F** adopts an arrangement of zigzag shape with a *J*-type aggregation of the molecules in the same column (Fig. 3a). Crystal **CMD-Cl** (Fig. S1†) has almost exactly the same intermolecular interactions and stacking arrangement as **CMD-F**. The difference is that the distances of the weak interactions in **CMD-Cl** are slightly longer than those in **CMD-F**, revealing that the former has the more loose arrangement than the latter. Although **CMD-Br** (Fig. S2†) has the same stacking arrangement as **CMD-F** and **CMD-Cl**, there exists a C–H···π bond with a distance of 2.611 Å between aromatic C–H and phenyl ring except C–H···O hydrogen bonds (2.500 and 2.650 Å), C–H···π (C=O) bond (2.666 Å), and π–π interaction (3.555 Å).

View Article Online
DOI: 10.1039/C9CE00348G

Table 2 The distances of the intermolecular interactions in crystals **CMD-H**, **CMD-F**, **CMD-Cl**, and **CMD-Br**

Crystal	Weak interaction	d/Å	Crystal	Weak interaction	d/Å
CMD-H	C28-H28A···π(Pyridine)	3.634	**CMD-F**	π(Pyridine)···π(Pyridine)	3.504
	C5-H5···π(Ph)	3.486		C15-H15···π(C=O)	2.616
	C1-H1···π(Pyridine)	3.614		C8-H8···N2	2.673
	C28-H28A···π(C=O)	2.459		C1-H1···N2	2.538
	C18-H18···H26A	2.391		C23-H23C···O2	2.709
	C18-H18···H25A	2.365		C17-H17···O1	2.718
	C18-H28A···H12	2.281		C21-H21···O1	2.375
	C18-H28A···O1	2.436		C15-H15···O1	2.624
CMD-Cl	π(Pyridine)···π(Pyridine)	3.561	**CMD-Br**	π(Pyridine)···π(Pyridine)	3.555
	C15-H15···π(C=O)	2.668		C15-H15···π(C=O)	2.666
	C6-H14···N2	2.830		C9-H9···π(Ph)	2.611
	C13-H13···N2	2.681		C17-H17··O1	2.500
	C21-H21···O1	2.814		C28-H28C···O2	2.650
	C17-H17···O1	2.470			
	C15-H15···O1	2.707			
	C28-H28A···O2	2.637			

As mentioned above, **CMD-H**, **CMD-F**, **CMD-Cl**, and **CMD-Br** have twisted molecular conformations, and their molecules are connected by various weak intermolecular interactions and adopt loose stacking arrangements. Based on these results, these compounds are expected to exhibit AIE and MFC properties.

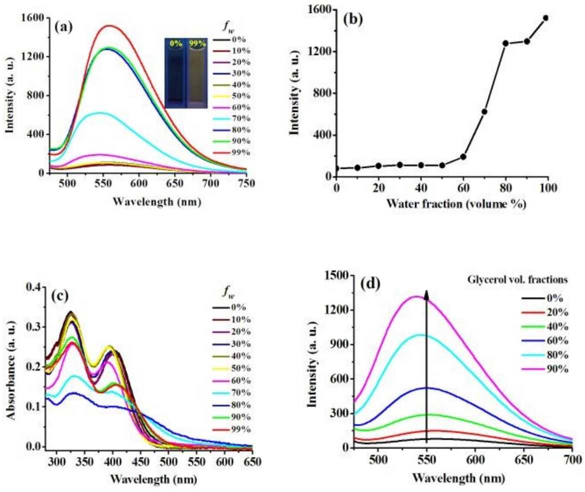

Fig. 4 **CMD-H**: Fluorescence spectra (a), changes in the fluorescence intensity (b), and UV-vis absorption spectra (c) in DMSO-water mixtures (10.0 μmol/L) with f_w = 0-99%. Fluorescence spectra (d) in DMSO-glycerol mixtures (10.0 μmol/L) with the glycerol volume fraction from 0 to 90%. The insets in (a) show digital photographs of the mixtures with f_w = 0 and 99% under a 365 nm ultraviolet lamp.

AIE properties

Considering that DMSO and water were good and poor solvents for the CMD derivatives, respectively, the UV-vis absorption and fluorescence spectra of these compounds in the DMSO-water mixtures by changing the volume percentage of water (f_w) in the range of 0-99% were investigated to determine whether they exhibited AIE properties. The DMSO-water mixtures (10.0 μmol/L) of **CMD-H** hardly emitted fluorescence when f_w was in the range of 0-50% (Fig. 4a and Fig. 4b). This should be attributed that the molecules with low volumetric ratios of water were dispersed and thus the free rotations of the phenyl rings greatly weakened the emissions through the non-radiative relaxation of the excited states.[11a,13] When the f_w value went up to 60-99%, the UV-vis absorption spectra of mixtures showed level-off tails in the long-wavelength region because of the Mie scattering effect (Fig. 4c), which indicated the formations of nanosized aggregates.[14] Correspondingly, the fluorescence intensity began to increase at f_w = 60% and reached the maximum at f_w = 99% which was 11-fold to that of the single-molecule state. The results indicated that the aggregation of the molecules led to the fluorescence enhancement, revealing that **CMD-H** was AIE-active molecule. To gain insights into the mechanism of AIE activity, the change of fluorescence spectra of **CMD-H** DMSO-glycerol mixtures (10.0 μmol/L) upon the varying glycerol volume fractions was conducted. It could be found that the increase of the glycerol volume fraction led to a gradual increase in fluorescence intensities of the mixtures (Fig. 4d). Because the glycerol was a liquid with high viscosity, the increase of glycerol volume fraction enhanced the viscosity of the mixtures, which prevented the free rotations of the phenyl rings and thus enhanced the fluorescence intesities.[15] The result indicated that the AIE activity of **CMD-H** was ascribed to the restriction of intramolecular rotation. Similarly, **CMD-F**, **CMD-Cl**, and **CMD-Br** also exhibited obvious AIE properties. Different from **CMD-H**, the fluorescence intensities of **CMD-F**, **CMD-Cl**, and **CMD-Br** exhibited a process of first enhancing and then weakening with the increasing f_w value. The strongest fluorescence intensity was observed at f_w = 70, 60, and 70% for **CMD-F** (Fig. S3†), **CMD-Cl** (Fig. S4†), and **CMD-Br** (Fig.

View Article Online
DOI: 10.1039/C9CE00348G

S5†), respectively. With the further increase of water content, the fluorescence intensity began to weaken gradually. Similar phenomena were often observed in some previously reported AIE-active molecules,[16] and the possible reason was that the dispersed molecules aggregated to form aggregates with different morphologies at higher f_w conditions.

MFC properties

The original samples of **CMD-H**, **CMD-Cl**, and **CMD-Br** exhibited yellow-green fluorescence with the λ_{em} values of 544, 529, and 533 nm, respectively, while that of **CMD-F** emitted green fluorescence with the λ_{em} value of 515 nm (Fig. 5 and Fig. 6). This indicated that the enhancement of electron-withdrawing ability of the substituent group could lead to the blue shift in the solid-state emission. As shown in Fig. 5, upon grinding in a mortar with a pestle, the original samples of these compounds were converted into orange-emitting solids. The 21, 60, 61, and 52-nm red-shift in the emission spectra were observed for **CMD-H**, **CMD-F**, **CMD-Cl**, and **CMD-Br**, respectively (Table 3). Although all these compounds exhibited MFC properties, obviously, the introduction of the halogen atoms resulted in higher contrast MFC phenomena. The XRD measurements of these compounds before and after grinding were conducted (Fig. 7). The original samples of these compounds exhibited a series of sharp and intense diffraction peaks, revealing the characteristics of crystalline state, whereas their ground samples were amorphous because of the disappearance of diffraction peaks. This indicated that the grinding treatment destroyed the crystalline structures of these compounds and led to a crystalline-to-amorphous transition in the morphologies. For **CMD-H**, after the ground sample was fumed by CH_3CN vapor, the sharp and intense diffraction peaks recovered, which accorded well with those of the XRD pattern of the original sample (Fig. 7a). This suggested that the fuming treatment resulted in a morphological change from the amorphous state to the crystalline state, and thus the recovery of fluorescence. As a result, the fumed sample emitted yellow-green fluorescence with the λ_{em} value of 544 nm, which was the same as the original sample (Fig. 6a). Similarly, the fuming treatment also recovered the fluorescence colours of the ground samples of the halogen-substituted CMD derivatives. As a result, a rewritable optical recording medium could be established based on **CMD-F** (Fig. 5e). When a picture containing a cat was painted on the surface of the original sample using a metal spatula, the orange picture appeared in the green background under a 365 nm UV lamp. Then, the picture was easily erased by fuming with CH_3CN vapor. However, it should be pointed out that for **CMD-F**, **CMD-Cl**, and **CMD-Br**, although most of the diffraction peaks of their fumed samples appeared again, the intensities were weaker than those of the corresponding original samples (Figs. 7b-7d), indicating that amorphous solids were partially present in the fumed samples.[6] Therefore, the λ_{em} values of their emissions could not be completely restored to the original states.

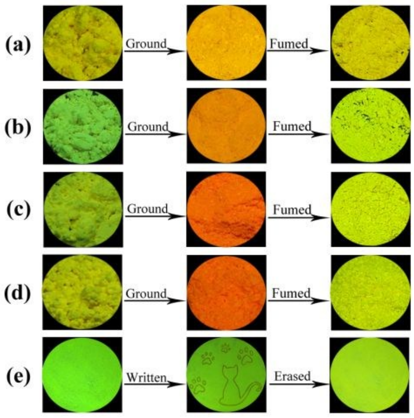

Fig. 5 Photographic images of the original samples of **CMD-H** (a), **CMD-F** (b), **CMD-Cl** (c), and **CMD-Br** (d) upon grinding and fuming (CH_3CN vapor) under irradiation at 365 nm. (e) A picture containing a cat was written and then erased based on the original sample of **CMD-F** under irradiation at 365 nm.

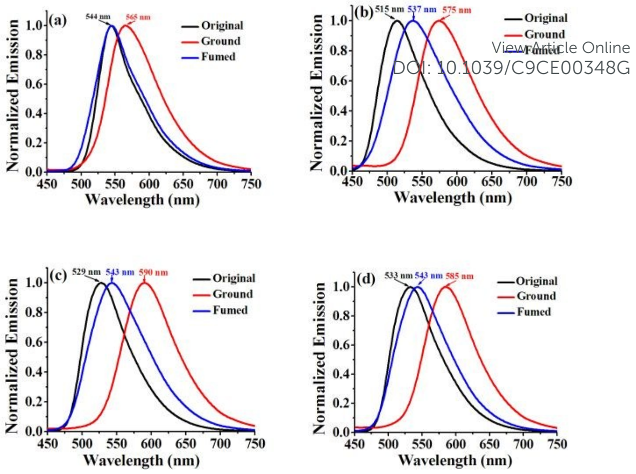

Fig. 6 Normalized fluorescence spectra of the original samples of **CMD-H** (a), **CMD-F** (b), **CMD-Cl** (c), and **CMD-Br** (d) upon grinding and fuming (CH_3CN vapor).

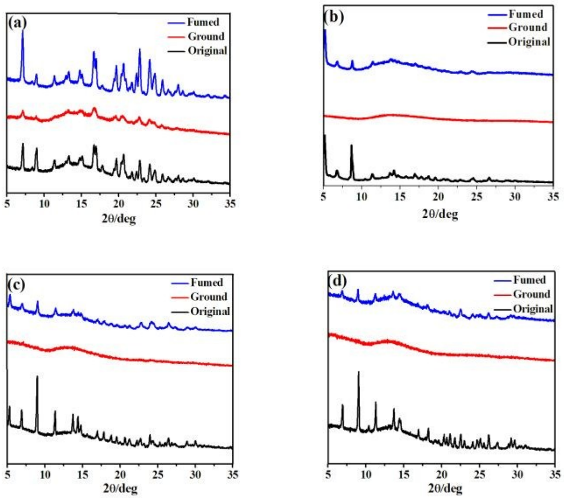

Fig. 7 XRD patterns of the original samples of **CMD-H** (a), **CMD-F** (b), **CMD-Cl** (c), and **CMD-Br** (d) upon grinding and fuming (CH_3CN vapor).

View Article Online
DOI: 10.1039/C9CE00348G

Table 3 Fluorescence parameters of the solid samples of **CMD-H**, **CMD-F**, **CMD-Cl**, and **CMD-Br**

Compound	Type	λ_{em} (nm)	τ_1 (ns)[a]	τ_2 (ns)[a]	A_1[b]	A_2[b]	<τ> (ns)[c]	Φ_F
CMD-H	Original	544	1.26	2.32	0.30	0.70	2.00	26.9%
	Ground	565	0.78	2.65	0.83	0.17	1.10	8.2%
	Fumed	544	0.95	2.89	0.74	0.26	1.45	10.8%
CMD-F	Original	515	0.06	2.35	0.82	0.18	2.37	21.3%
	Ground	575	0.62	2.44	0.94	0.06	0.73	4.4%
	Fumed	539	0.06	2.16	0.83	0.17	1.28	11.3%
CMD-Cl	Original	529	0.11	3.26	0.29	0.71	2.35	26.5%
	Ground	590	0.93	3.37	0.90	0.10	1.17	3.0%
	Fumed	543	0.84	3.73	0.53	0.47	2.20	12.5%
CMD-Br	Original	533	0.16	2.78	0.17	0.83	2.33	25.1%
	Ground	585	0.53	2.79	0.90	0.10	0.76	4.6%
	Fumed	543	0.35	2.56	0.29	0.71	1.92	13.8%

[a] Fluorescence lifetime. [b] Proportion. [c] Weighted mean lifetime <τ> was determined from <τ> = $(A_1\tau_1+A_2\tau_2)/(A_1+A_2)$.

The fluorescence quantum yields (Φ_F) and the time-resolved fluorescence decay parameters of the CMD derivatives in different solid states were investigated and shown in Table 3. The Φ_F values of the original samples of **CMD-H**, **CMD-F**, **CMD-Cl**, and **CMD-Br** were 26.9, 21.3, 26.5, and 25.1%, whereas those of the corresponding ground samples were 8.2, 4.4, 3.0, and 4.6%, respectively, indicating that the grinding process could reduce the efficiency of fluorescence quantum yields. This should be attributed that grinding destroyed the intermolecular interactions in the *J*-aggregation and enhanced the non-radiative relaxations. Additionally, the weighted mean lifetime (<τ>) values of the original samples of **CMD-H**, **CMD-F**, **CMD-Cl**, and **CMD-Br** were 2.00, 2.37, 2.35, and 2.81 ns, whereas those of their corresponding ground samples were 1.10, 0.73, 1.17, and 0.76 ns, revealing that the grinding treatment caused a significant decrease in <τ> values. Interestingly, in the case of previously reported MFC-active 1,4-dihydropyridine derivatives, the <τ> values often increased significantly after grinding.[11b,e] Although the reasons for this opposite trend were not yet clear, there was no doubt that external pressure could lead to remarkable changes in <τ> values for MFC-active organic compounds.

According to the single crystal structures of the CMD derivatives, we can better understand the intrinsic reasons for the generation of MFC derivatives of the CMD derivatives. As shown in Fig. S6†, the diffraction peaks of the CMD derivatives original samples in the XRD patterns accorded well with the simulated peaks of the corresponding single crystals, indicating that the original samples should have the same stacking arrangements as the single crystals.[17] Upon grinding, the loose *J*-aggregations with the weak intermolecular interactions in the original samples were easily destroyed, which resulted in the morphological changes from a crystalline state to an amorphous state and thus the MFC properties of these compounds.

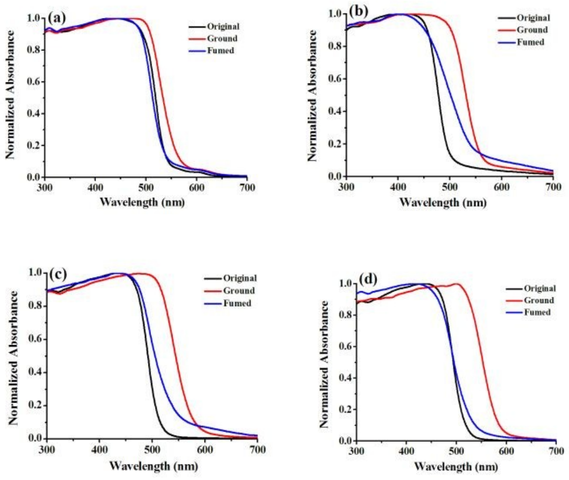

Fig. 8 Normalized absorption spectra of the original samples of **CMD-H** (a), **CMD-F** (b), **CMD-Cl** (c), and **CMD-Br** (d) upon grinding and fuming (CH_3CN vapor).

Why did the introduction of halogen atoms help to enhance the MFC activities? Possible reasons for this phenomenon were listed as follows. As shown in Table 2, the distances of the intermolecular interactions in **CMD-H** were generally shorter than those in **CMD-F**, **CMD-Cl**, and **CMD-Br**. Futhermore, the herringbone angle in the zigzag arrangement of **CMD-H** was 115° (Fig. 2), while that in halogen-substituted CMD derivatives was about 133° (Fig. 3, Fig. S1†, and Fig. S2†), suggesting that the latter had looser arrangements. The weaker intermolecular interactions and looser arrangements caused that the original samples of the halogen-substituted CMD derivatives were more easily destroyed, and thus the diffraction peaks in their XRD curves completely disappeared upon grinding, while few broad and weak peaks remained in the XRD curve of the **CMD-H** ground sample (Fig. 7). Generally, the red shift in the emission spectrum upon grinding may originate from the formation of excimers induced by the enhancement of the π–π interactions or the increased molecular conjugation caused by the planarization of molecular conformation. According to the report of

View Article Online
DOI: 10.1039/C9CE00548G

Chi's group[18], if the red shift of the emission spectrum was caused by the formation of excimers, the maximum absorption peaks should remain unchanged, while the increased molecular conjugation could lead to outstanding changes. Upon grinding, the CMD derivatives original samples all exhibited obvious red shifts in the maximum absorption peaks (Fig. 8), indicating that the red shifts of emission wavelengths in these cases should be mainly ascribed to the enhancement of the molecular conjugation. As described above, **CMD-F**, **CMD-Cl**, and **CMD-Br** had more twisted conformations than **CMD-H**, so their molecules had more space for change in the process of the planarization of molecular conformation after grinding, thus showing greater red shifts in the emission spectra. The results indicated that more twisted conformations and looser stacking arrangements could be used to explain the reason why the introduction of the halogen atoms led to the enhanced MFC phenomena.

Conclusions

In conclusion, we synthesized four AIE-active CMD derivatives and found the introduction of halogen atoms led to the enhanced MFC activities. These compounds had twisted molecular conformations and adopted loose *J*–aggregations, which caused that their crystalline structures were easily destroyed by the grinding treatment. Their MFC properties were demonstrated to originate from the crystalline-to-amorphous transition and the red shifts of emission wavelengths were ascribed to the enhancement of the molecular conjugations through the planarization of molecular conformations. Compared with **CMD-H**, the introduction of halogen atoms led to more twisted conformations and looser stacking arrangements of **CMD-F**, **CMD-Cl**, and **CMD-Br**, which was responsible for their higher contrast MFC properties. The results indicated that the introduction of halogen atoms into a specific traditional fluorescent molecule may contribute to the formation of high contrast MFC fluorescent materials.

Acknowledgements

We thank the National Natural Science Foundation of China (Nos 21572165 and 21472140) and the Xinmiao Foundation of Zhejiang Province (No 2018R429057) for financial support.

Notes and references

1 (a) Z. Chi, X. Zhang, B. Xu, X. Zhou, C. Ma, Y. Zhang, S. Liu and J. Xu, *Chem. Soc. Rev.*, 2012, **41**, 3878–3896; (b) Y. Sagara, S. Yamane, M. Mitani, C. Weder and T. Kato, *Adv. Mater.*, 2016, **28**, 1073–1095.

2 Y. Sagara, T. Mutai, I. Yoshikawa and K. Araki, *J. Am. Chem. Soc.*, 2007, **129**, 1520–1521.

3 (a) X. Huang, L. Qian, Y. Zhou, M. Liu, Y. Cheng and H. Wu, *J. Mater. Chem. C*, 2018, **6**, 5075–5096; (b) Z. Yang, Z. Chi, Z. Mao, Y. Zhang, S. Liu, J. Zhao, M. P. Aldred and Z. Chi, *Mater. Chem. Front.*, 2018, **2**, 861–890; (c) C. Wang and Z. Li, *Mater. Chem. Front.*, 2017, **1**, 2174–2194; (d) J. Zhao, Z. Chi, Z. Yang, Z. Mao, Y. Zhang, E. Ubba and Z. Chi, *Mater. Chem. Front.*, 2018, **2**, 1595–1608; (e) Y. Dong, J. W. Y. Lam and B. Z. Tang, *J. Phys. Chem. Lett.*, 2015, **6**, 3429–3436; (f) J. Zhao, Z. Chi, Y. Zhang, Z. Mao, Z. Yang, E. Ubba and Z. Chi, *J. Mater. Chem. C*, 2018, **6**, 6327–6353; (g) S. Mukherjee and P. Thilagar, *J. Mater. Chem. C*, 2016, **4**, 2647–2662; (h) Z. Ma, Z. Wang, M. Teng, Z. Xu and X. Jia, *ChemPhysChem*, 2015, **16**, 1811–1828; (i) S. Xue, X. Qiu, Q. Sun and W. Yang, *J. Mater. Chem. C*, 2016, **4**, 1568–1578.

4 S. Varghese and S. Das, *J. Phys. Chem. Lett.*, 2011, **2**, 863–873.

5 P. Xue, B. Yao, J. Sun, Q. Xu, P. Chen, Z. Zhang and R. Lu, *J. Mater. Chem. C*, 2014, **2**, 3942–3950.

6 P. Rajamalli, P. Gandeepan, M. J. Huang and C. H. Cheng, *J. Mater. Chem. C*, 2015, **3**, 3329–3335.

7 C. Ma, X. Zhang, Y. Yang, Z. Ma, L. Yang, Y. Wu, H. Liu, X. Jia and Y. Wei, *Dyes Pigm.*, 2016, **129**, 141–148.

8 Y. Qi, Y. Wang, Y. Yu, Z. Liu, Y. Zhang, G. Du and Y. Qi, *RSC Adv.*, 2016, **6**, 33755–33762.

9 W. A. Morris, T. Liu and C. L. Fraser, *J. Mater. Chem. C*, 2015, **3**, 352–363.

10 (a) Z. Guo, A. Shao and W. Zhu, *J. Mater. Chem. C*, 2016, **4**, 2640–2646; (b) C. Shi, Z. Guo, Y. Yan, S. Zhu, Y. Xie, Y. Zhao, W. Zhu and H. Tian, *ACS Appl. Mater. Interfaces*, 2013, **5**, 192−198.

11 (a) H. Li, Y. Guo, G. Li, H. Xiao, Y. Lei, X. Huang, J. Chen, H. Wu, J. Ding and Y. Cheng, *J. Phys. Chem. C*, 2015, **119**, 6737−6748; (b) Y. Lei, Y. Liu, Y. Guo, J. Chen, X. Huang, W. Gao, L. Qian, H. Wu, M. Liu and Y. Cheng, *J. Phys. Chem. C*, 2015, **119**, 23138−23148; (c) Y. Lei, Y. Lai, L. Dong, G. Shang, Z. Cai, J. Shi, J. Zhi, P. Li, X. Huang, B. Tong and Y. Dong, *Chem. Eur. J.*, 2018, **24**, 434−442; (d) Y. Lei, D. Yang, H. Hua, C. Dai, L. Wang, M. Liu, X. Huang, Y. Guo, Y. Cheng and H. Wu, *Dyes Pigm.*, 2016, **133**, 261−272; (e) Y. Liu, Y. Lei, M. Liu, F. Li, H. Xiao, J. Chen, X. Huang, W. Gao, H. Wu and Y. Cheng, *J. Mater. Chem. C*, 2016, **4**, 5970−5980; (f) Y. Zhou, L. Qian, M. Liu, X. Huang, Y. Wang, Y. Cheng, W. Gao, G. Wu and H. Wu, *J. Mater. Chem. C*, 2017, **5**, 9264−9272; (g) M. Wang, L. Qian, Y. Guo, H. Wu, M. Liu, W. Gao, G. Li, J. Ding and X. Huang, *Dyes Pigm.*, 2019, **160**, 378–385.

12 G. Kwak, S. Wang, M. S. Choi, H. Kim, K. H. Choi, Y. S. Han, Y. Hur and S. H. Kim, *Dyes Pigm.*, 2008, **78**, 25–33.

13 J. Luo, Z. Xie, J. W. Y. Lam, L. Cheng, H. Chen, C. Qiu, H. S. Kwok, X. Zhan, Y. Liu, D. Zhu and B. Z. Tang, *Chem. Commun.*, 2001, 1740–1741.

14 H. Auweter, H. Haberkorn, W. Heckmann, D. Horn, E. Lüddecke, J. Rieger and H. Weiss, *Angew. Chem., Int. Ed.*, 1999, **38**, 2188–2191.

15 J. Chen, C. C. W. Law, J. W. Y. Lam, Y. Dong, S. M. F. Lo, I. D. Williams, D. Zhu and B. Z. Tang, *Chem. Mater.*, 2003, **15**, 1535–1546.

16 (a) X. Zhang, Z. Chi, B. Xu, C. Chen, X. Zhou, Y. Zhang, S. Liu and J. Xu, *J. Mater. Chem.* 2012, **22**, 18505–18513; (b) X. Zhang, Z. Yang, Z. Chi, M. Chen, B. Xu, C. Wang, S. Liu, Y. Zhang and J. Xu, *J. Mater. Chem.*, 2010, **20**, 292−298; (c) Y. Dong, J. W. Y. Lam, A. Qin, J. Sun, J. Liu, Z. Li, J. Z. Sun, H. H. Y. Sung, I. D. Williams, H. S. Kwok and B. Z. Tang, *Chem. Commun.*, 2007, 3255−3257; (d) Q. Lu, X. Li, J. Li, Z. Yang, B. Xu, Z. Chi, J. Xu and Y. Zhang, *J. Mater. Chem. C*, 2015, **3**, 1225–1234.

17 J. Chen, S. Ma, J. Zhang, L. Wang, L. Ye, B. Li, B. Xu and W. Tian, *J. Phys. Chem. Lett.*, 2014, **5**, 2781−2784.

18 X. Zhang, Z. Chi, X. Zhou, S. Liu, Y. Zhang, and J. Xu, *J. Phys. Chem. C*, 2012, **116**, 23629−23638.

View Article Online
DOI: 10.1039/C9CE00348G

Enhanced mechanofluorochromic properties of 1,4-dihydropyridine-based fluorescence molecules caused by the introduction of halogen atoms

Yating Chen, Yibin Zhou, Zhiqiang Wang, Mengzhu Wang, Wenxia Gao, Yunbing Zhou, Miaochang Liu, Xiaobo Huang and Huayue Wu

The halogen-substituted 1,4-dihydropyridine derivatives exhibit higher contrast mechanofluorochromic properties than the derivative without the halogen atom because of more twisted conformations and looser stacking arrangements.